

Uni6Dv3: 5D Anchor Mechanism for 6D Pose Estimation

Jianqiu Chen*,¹ Mingshan Sun*,² Ye Zheng,¹ Tianpeng Bao,² Zhenyu He†,¹ Donghai Li,²
Guoqiang Jin,² Rui Zhao,² Liwei Wu,² Xiaoke Jiang²

¹ Harbin Institute of Technology, Shenzhen

² SenseTime Research

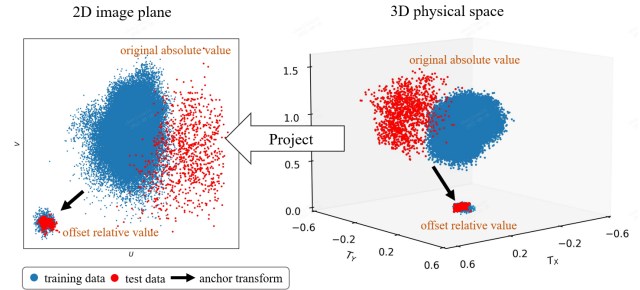
³ Institute of Computing Technology, Chinese Academy of Sciences

Abstract

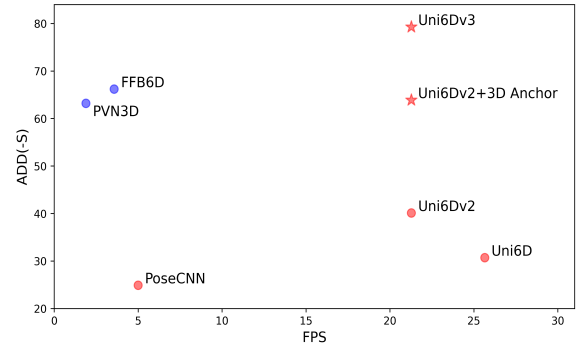
Unlike indirect methods that usually require time-consuming post-processing, recent deep learning-based direct methods for 6D pose estimation try to predict the 3D rotation and 3D translation from RGB-D data directly. However, direct methods, regressing the absolute translation of the pose, suffer from diverse object translation distribution between training and test data, which is usually caused by expensive data collection and annotation in practice. To this end, we propose a 5D anchor mechanism by defining the anchor with 3D coordinates in the physical space and 2D coordinates in the image plane. Inspired by anchor-based object detection methods, 5D anchor regresses the offset between the target and anchor, which eliminates the distribution gap and transforms the regression target to a small range. But regressing offset leads to the mismatch between the absolute input and relative output. We build an **anchor-based projection model** by replacing the absolute input with the relative one, which further improves the performance. By plugging 5D anchor into the latest direct methods, Uni6Dv2 and ES6D obtain 38.7% and 3.5% improvement, respectively. Specifically, Uni6Dv2+5D anchor, dubbed **Uni6Dv3**, achieves state-of-the-art overall results on datasets including Occlusion LineMOD (79.3%), LineMOD (99.5%), and YCB-Video datasets (91.5%), and requires only 10% of training data to reach comparable performance as full data.

Introduction

6D pose estimation has drawn widespread attention since it is the essential prerequisite of emerging applications such as robotic manipulation, autonomous driving, and augmented reality (Geiger, Lenz, and Urtasun 2012; Xu, Anguelov, and Jain 2018; Chen et al. 2017). Estimating 6D pose from RGB-D data has been a common practice thanks to the affordable RGB-D sensor. We have witnessed significant progress driven by the deep learning approach for 6D pose estimation, be it indirect or direct methods. Indirect methods (He et al. 2020, 2021) usually predict an intermediate result first, then use the post-processing optimization algorithm, such as clustering and iterative Perspective-n-Point (PnP) algorithms (Su et al. 2022; Haugaard and Buch 2022; Li, Wang,



(a) Distribution of object centers (T) on Occlusion LineMOD: 1) distribution of T between training and test data is diversely distributed in a wide range; 2) 5D anchor can transform T to a more compact distribution.



(b) Comparison of speed and accuracy on the Occlusion LineMOD: Uni6Dv3 achieves state-of-the-art accuracy in both direct (red dots) and indirect (blue dots) methods. 3D Anchor stands for applying offset only in target without in input data.

Figure 1: Design of 5D anchor and its performance comparison of accuracy and speed.

and Ji 2019; Kiru, Patten, and Pix2Pose 2019; Rad and Lepetit 2017), to calculate the final result, whereas the direct methods (Mo et al. 2022a; Jiang et al. 2022; Li et al. 2018; Wang et al. 2020, 2021; Sun et al. 2022; Mo et al. 2022b) predict the final 6D pose directly without post-processing, i.e., in an end-to-end manner. It's worth noting that recent direct methods (Jiang et al. 2022; Sun et al. 2022) reveal a

*These authors contributed equally.

†Corresponding author

critical characteristic of the 6D pose estimation task: its input and output should follow the projection equation since the depth image holds the 3D structure of the object, which is transformed by the rotation and translation in 3D space.

However, there is still room for performance improvement of direct methods, especially on the challenging datasets with diverse translation distribution of objects, such as Occlusion LineMOD (Brachmann et al. 2014). As shown in Fig. 1(a), the translation T between training and test data is *diversely* distributed in a *wide* range. Here we take ‘‘egg-box’’ from the Occlusion LineMOD as an example, original T_x range in $(-0.33, 0.29)$ and $(-0.11, 0.61)$ in training and test data, respectively. The widely distributed T would increase network convergence’s difficulty and require more training data for the network to converge. Inevitably, diverse distribution between training and test data, which greatly harms the accuracy, is quite common in practice due to the expensive data collection and annotation. Furthermore, the direct methods directly predict the final result, other than the indirect methods that can use the intermediate results as the relative information. Thus, the direct methods would be more vulnerable to distribution gaps.

Revisiting the object detection field (He et al. 2017), anchor is adopted to convert the absolute location regression target into the offset (relative value) to the anchor box, which decouples the network regression target with object location. Intuitively, we could change the regression target T to be the offset of the object’s translation to a given anchor, which is represented by 3D coordinates (x_0, y_0, d_0) in the physics world. In this way, the reshaped regression target (offset of T) could eliminate the domain gap and scatters in a small range, as shown in Fig. 1(a). Offset of eggbox’s T_x is range in $(-0.07, 0.07)$ and $(-0.05, 0.06)$ in training and test data, respectively. However, the input and corresponding target no longer hold the aforementioned projection equation, leading to the mismatch between the input and its output.

To this end, we extend the projection equation (Eq.1) to the situation with anchor and build **anchor-based projection model** (more details in Sec. Methodology) to rebalance the input and output of the task. According to the model, we also replace the absolute input information with the relative value from the anchor. Besides x_0, y_0, d_0 , the replaced input includes u_0, v_0 that appear in the new projection model. Therefore, our anchor has 5 elements in total, i.e., $(u_0, v_0, x_0, y_0, d_0)$. We name it the 5D anchor, which is shown in Fig. 2. Different from that classical anchors that only consider the output, 5D anchor adjust the output and input simultaneously based on the anchor-based projection equation. We plug 5D anchor to direct methods Uni6Dv2 and ES6D, and obtain 38.7% and 3.5% improvement w.r.t ADD(S), respectively.

Specifically, Uni6D series (Jiang et al. 2022; Sun et al. 2022) create a promising paradigm that enable a single CNN backbone to handle RGB-D images and predicts 6D pose directly in the end-to-end style without post-processing. We apply the 5D anchor to the latest Uni6Dv2 and obtain a new method Uni6Dv3, which outperforms all existing 6D pose estimation methods on YCB-Video, LineMOD, and Occlusion LineMOD datasets. The overall performance on

the three datasets obtains 3.9% compared to state-of-the-art method (He et al. 2021). The performance gain is obvious on the most challenging dataset, occlusion LineMOD, as shown in Fig. 1(b), Uni6Dv3 achieves 38.7% performance improvement compared to Uni6Dv2 (Sun et al. 2022) and outperforms the indirect state-of-the-art method (He et al. 2021) by 13.1% w.r.t ADD(S) metric. Furthermore, after being transformed by the 5D anchor, the object distribution becomes compact, thus reducing the difficulty of network convergence, which greatly reduces the dependency on the data. It only requires 10% of training data and reaches comparable performance (1.7% and 5% decrease w.r.t ADD-S and ADD(S), respectively, Table 6). To summarize, our main contributions are:

- **Anchor-based projection model:** To the best of our knowledge, we are the first to uncover the input and output mismatch issue, besides the advantages of introducing anchor to the task. And we build an anchor-based projection model to solve this issue.
- **5D anchor mechanism:** we propose 5D anchor to solve the translation distribution problem in 6D pose estimation task by adjusting the regression target and its input simultaneously. 5D anchor is proved to work with different direct 6D pose estimation methods.
- **Uni6Dv3:** We propose Uni6Dv3, which outperforms all existing 6D pose estimation methods while significantly reducing data requirements. Worth noting that Uni6Dv3 also maintains both simplicity and efficiency.

Related Work

We review the indirect and direct methods in 6D pose estimation and different anchor mechanisms in this section.

Projection Equation in 6D Pose Estimation

6D pose estimation is the task of predicting the rotation and translation from object coordinate system to camera coordinate system based on RGB-D image. Each visible point on the surface of 3D object is projected to RGB-D image following the projection equation

$$\begin{bmatrix} u \\ v \\ 1 \end{bmatrix} = \frac{K}{d} \begin{bmatrix} x \\ y \\ d \end{bmatrix} = \frac{K}{R_z(a, b, c) + T_z} \left(R \times \begin{bmatrix} a \\ b \\ c \end{bmatrix} + T \right), \quad (1)$$

where a point (a, b, c) in the object coordinate system is first rotated and translated by R and T to the position (x, y, d) in the camera coordinate system, then it is projected to the pixel at (u, v) in the image plane through the intrinsic matrix K of the camera.

The current deep learning-based 6D pose estimation consists of indirect and direct methods. The former regresses an intermediate geometric representation and then estimates the 6D pose by an optimization function, while the latter predicts the final 6D pose directly.

Indirect method

Indirect methods first predict intermediate geometric information, such as *keypoints* in camera coordinate or *2D-3D*

correspondence, and then exploit the projection constraints to estimate the 6D pose by optimization function.

Keypoint-based methods: PVNet (Peng et al. 2019a) is the pioneer in introducing the keypoints mechanism in 6D pose estimation; it adopts a voting network to densely regress the predefined 2D keypoints of objects and then estimate the 6D pose by an uncertainty-driven PnP algorithm. Recent methods (He et al. 2020, 2021) extend the 2D keypoints to 3D space by regressing the predefined 3D keypoints of objects and estimating the 6D pose by a least-squares fitting algorithm. In order to obtain accurate 3D keypoints, the network regresses the offsets of visible points to the 3D keypoints and then uses an iterative voting mechanism to vote for the best prediction.

Correspondence-based methods: Different from the keypoints-based methods, 2D-3D correspondence-based methods (Su et al. 2022; Hodan, Barath, and Matas 2020; Haugaard and Buch 2022; Li, Wang, and Ji 2019; Kiru, Paten, and Pix2Pose 2019; Rad and Lepetit 2017) first establish the correspondence between 2D coordinates in the image plane and 3D coordinates in the object coordinate system by neural network, and then solve the 6D pose by a PnP or RANSAC algorithm. The 2D-3D correspondence usually can be regarded as a classification task or 3D points regression task; outputs of these tasks are usually in a small range so that the network learning is easier. However, both keypoints and correspondences are only optimized in the first stage rather than the final pose regression, which is suboptimal compared with direct methods. More importantly, the iterative voting and optimization are time-consuming and heavy in practical applications.

Direct method

To estimate 6D pose efficiently, recent approaches (Mo et al. 2022a; Jiang et al. 2022; Li et al. 2018; Wang et al. 2020, 2021) directly regress the final 6D pose parameters instead of intermediate results. Densefusion (Wang et al. 2019) extract geometric and appearance information from RGB-D images individually and fuse them by a dense fusion network. Yet, the heterogeneous architecture is still heavy in practical applications. Uni6D series (Jiang et al. 2022; Sun et al. 2022) simplify the architecture by a single backbone. Uni6D (Jiang et al. 2022) exposes the projection breakdown problem of processing depth image in the CNN framework and first leverages a single homogeneous backbone to process RGB-D data, introducing the extra UV data into input to preserve the projection constraint. In the following work uni6Dv2 (Sun et al. 2022), a two-step denoising approach is proposed to guide the network to learn the object-relevant feature and calibrate depth information. However, it is challenging to directly regress the absolute translation because the output space is theoretically infinite, especially when there is a distribution gap between training and test dataset. To alleviate the aforementioned problem, ES6D (Mo et al. 2022a) densely regresses offsets from visible points to the centroid point in 3D space. However, the mismatch between the input and output limits the accuracy of pose estimation.

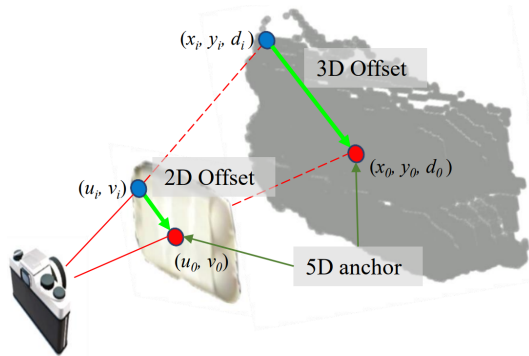


Figure 2: Demonstration of 5D anchor. Red dots denote 5D anchor and Blue dots denote a visible point

Anchor mechanism

2D anchor is mainly used in 2D detection tasks (Ren et al. 2015), it simplifies the absolute box location as the offset of center point (x_c, y_c) , width w and height h for anchor box. The inputs are usually the RGB images. Similarly, some 3D detection methods (Zhou and Tuzel 2018; Lang et al. 2019) extend the 2D anchor into 3D space, building a 3D anchor box including seven elements: the center point (x_c, y_c, z_c) , the width w , height h , length l and yaw angle θ of the anchor box. In addition, PVN3D and FFB6D (He et al. 2020, 2021) in 6D pose estimation take the similar operation to regress the offsets of visible points and predefined 3D keypoints. The above anchor mechanisms compact output distribution and decrease the difficulty of network convergence. However, it has a potential pitfall for the 6D pose estimation task: the mismatch between absolute input and relative output, which breaks the projection equation and severely limits the performance. Hence, we propose the 5D anchor in the 2D image plane and 3D space. Unlike the keypoint-based pose estimation method to regress the offset of visible points to keypoints, we regress the offset of anchor to centroid to predict the final pose directly. Mostly, based on the anchor-based projection model, we overcome the mismatch problem by introducing an extra 2D coordinate of the anchor to input.

Methodology: 5D Anchor and Uni6Dv3

In this section, we first give a short review of the classical Uni6D series, Uni6D (Jiang et al. 2022) and Uni6Dv2 (Sun et al. 2022). Then present the anchor-based projection model and 5D anchor, and lastly, we present the design of Uni6Dv3.

Review of Uni6D and Uni6Dv2

Uni6D (Jiang et al. 2022) is the first to achieve using a unified CNN backbone to handle both RGB image and depth data by adding the UV information into the input to solve the projection breakdown issue. The architecture of Uni6D is inherited from Mask RCNN (He et al. 2017), and employs RT head for directly predicting 6D pose and an auxiliary abc head for guiding the network to map the visible points

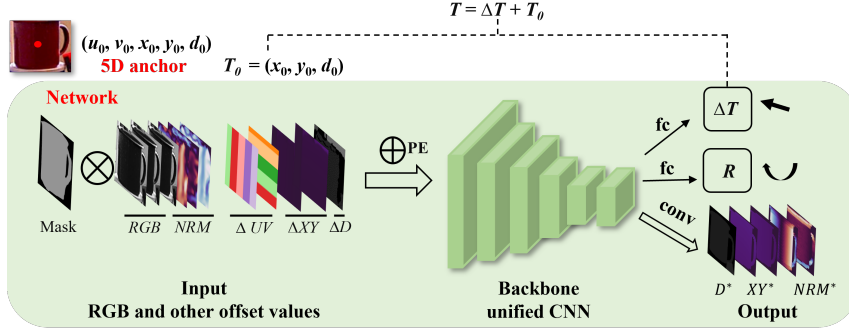


Figure 3: The architecture of Uni6Dv3. The absolute input is converted to offset by 5D anchor, and the final translation T is calculated by adding the anchor position T_0 with predicted offsets ΔT . “PE” is the position encoding.

to their coordinates in the 3D model. Since all the visible points’ data (U, V, X, Y, D to represent 2D and 3D coordinates of all visible points) and R, T satisfy the projection equation, Uni6D add U, V, X, Y to the input together with D .

Uni6Dv2 (Sun et al. 2022) focuses on the denoising issue during 6D pose estimation. It decouples the object detection from pose estimation and proposes a two-step pipeline. In the first step, it uses an instance segmentation network to crop and mask the instance to remove noise from non-instance regions. In the second step, a lightweight depth denoising module is proposed to calibrate the depth feature before feeding it into the pose regression network.

In both Uni6D and Uni6Dv2, the pose estimation task can be formulated as the follows:

$$R, T = f(RGB, U, V, X, Y, D, NRM), \quad (2)$$

where RGB and NRM are the color and depth normal vector of visible points for target objects, respectively.

5D Anchor and Anchor-based Projection

As shown in Eq 3, the 5D anchor is a predefined point (red dot in Fig2) in both 2D image plane and 3D physical space, which consists of 5 elements $(u_0, v_0, x_0, y_0, d_0) \in (U, V, X, Y, D)$ and satisfies the following projection equation:

$$\begin{bmatrix} u_0 \\ v_0 \\ 1 \end{bmatrix} = K \begin{bmatrix} x_0 \\ d_0 \\ y_0 \\ d_0 \\ 1 \end{bmatrix} = K \left(R \times \begin{bmatrix} a_0 \\ d_0 \\ b_0 \\ d_0 \\ c_0 \\ d_0 \end{bmatrix} + \frac{(T-T_0)}{d_0} + \frac{T_0}{d_0} \right), \quad (3)$$

where T_0 denotes the position (x_0, y_0, d_0) of 5D anchor in 3D space of camera coordinate system. According to Eq 1 and Eq 3, both sides of the projection equation subtract the 2D coordinates (u_0, v_0) and 3D coordinates (x_0, y_0, d_0) respectively. The projection constraint about a visible point $(u_i, v_i, x_i, y_i, d_i)$ and 5D anchor is reformulated in relative value reference to the 5D anchor, named it anchor-based projection as Eq 4, denoted as follows:

$$\begin{bmatrix} \Delta u \\ \Delta v \\ 0 \end{bmatrix} = K \begin{bmatrix} \Delta x \\ \Delta y \\ 0 \end{bmatrix} = K \left(R \times \begin{bmatrix} a_i - a_0 \\ d_i - d_0 \\ b_i - b_0 \\ d_i - d_0 \\ c_i - c_0 \\ d_i - d_0 \end{bmatrix} - \frac{\Delta d(\Delta T + T_0)}{d_i d_0} \right), \quad (4)$$

where

$$\begin{aligned} \Delta u &= u_i - u_0, \Delta v = v_i - v_0, \\ \Delta x &= \frac{x_i}{d_i} - \frac{x_0}{d_0}, \Delta y = \frac{y_i}{d_i} - \frac{y_0}{d_0}, \\ \Delta d &= d_i - d_0, \Delta T = T - T_0. \end{aligned}$$

Compared with the wide range and incompact distribution of T , the optimization target ΔT is formulated in relative offset, which distributes in a narrow range between $-r$ to r , and r is the radius of the object. Because the object shape is known and fixed, the distribution of ΔT is invariant and decoupled with the absolute positions of the object. Following Anchor-based Projection, we adjust the input into offset reference to 5D anchor. The pose estimation with anchor could be reformulated as:

$$R, \Delta T = f'(RGB, \Delta U, \Delta V, \Delta X, \Delta Y, \Delta D, NRM). \quad (5)$$

Design of Uni6Dv3

We follow the framework of Uni6Dv2, using the ROI cropped and masked by the instance segmentation network as the input of the regression network, which is illustrated in Fig. 3.

5D anchor generation. Establishing a stable 5D anchor can make data distribution uniform and compact, helping the network to learn the 6D pose. Based on the input data, we select the ROI center 2D coordinate as the (u, v) value in 5D anchor, and then leverage the (u, v) and mean depth of object pixels to calculate (x, y, d) values of 5D anchor following the projection equation. This generation strategy holds a stable anchor on the 2D image plane and makes the anchor as much as possible close to the origin of the object in 3D space.

Network architecture. After obtaining the predefined 5D anchor, we calculate the varies of offsets according to the Eq 4. Afterward, we combine RGB image, depth normal, and corresponding offsets data along the channel dimension, and input them into the backbone and depth denoising model to extract features. Significantly, compared with the absolute input, the features in our method will keep equality in different positions, which conforms to the translation invariance of convolution. Finally, the outputs of the network include

the rotation matrix in the form of quaternion, translation offset, re-projected XYD , and NRM for depth denoising.

Loss function. Our overall objective function is composed of 6D pose estimation terms and depth denoising terms. The 6D pose regression loss \mathcal{L}_{pose} is defined as:

$$\mathcal{L}_{pose} = \frac{1}{m} \sum_{x \in \mathcal{O}} \|(Rx + T_0 + \Delta T - (R^*x + T^*))\|, \quad (6)$$

where \mathcal{O} denotes the set of object’s points from the 3D model, R and T are the rotation matrix and the translation vector, m is the number of points in \mathcal{O} and $*$ denotes the ground truth. We follow the Uni6D framework to alleviate the depth noise, and the depth denoising loss is:

$$L_{depth} = |d - d^*| + |x - x^*| + |y - y^*| + |n_x - n_x^*| + |n_y - n_y^*| + |n_z - n_z^*|, \quad (7)$$

where d is the predicted depth and (n_x, n_y, n_z) is the regressed depth normal, (x, y) is the predicted visible point’s coordinate in the camera coordinate system. Finally, the overall loss function of our method is:

$$\mathcal{L} = \lambda_0 \mathcal{L}_{pose} + \lambda_1 \mathcal{L}_{depth}, \quad (8)$$

where λ_0 and λ_1 are the weights for each loss.

Experiments

Benchmark Datasets

We conduct our experiments on three benchmark datasets.

LineMOD (Hinterstoisser et al. 2011) contains 13 sequences of 13 low-textured objects. Since there is only about 1.2k real training data annotated with 6D pose, we follow previous work (Peng et al. 2019b; Xiang et al. 2018; He et al. 2020; Jiang et al. 2022) to add synthetic images for training with 99.71% synthetic ratio.

Occlusion LineMOD (Brachmann et al. 2014) consists of 1214 testing images which are selected from the LineMOD dataset in occlusion scene. Since there is no extra real training data, the training dataset is same as LineMOD. The domain gap between training and testing datasets, as well as the heavily occluded objects, make it more challenging for 6D pose estimation.

YCB-Video (Calli et al. 2015) is a large and challenging dataset which contains 21 objects with 92 RGB-D sequences. It provides a large amount of real training data holding the same pose distribution between training and testing datasets.

Evaluation Metrics

We adopt the commonly used average distance metrics ADD, ADD-S and ADD(S) to evaluate different methods. ADD evaluates the mean of pairwise distance between two object point clouds which are transformed according to the predicted pose $[R, T]$ and ground truth pose $[R^*, T^*]$ respectively:

$$\text{ADD} = \frac{1}{m} \sum_{x \in \mathcal{O}} \|(Rx + T) - (R^*x + T^*)\| \quad (9)$$

where \mathcal{O} denotes the 3D model of a object, x denotes any point on the model and m denotes total point number in the model. To alleviate the ambiguous matching of the symmetric objects, ADD-S is adopted to estimate the closest point distance between two point clouds:

$$\text{ADD-S} = \frac{1}{m} \sum_{x_1 \in \mathcal{O}} \min_{x_2 \in \mathcal{O}} \|(Rx_1 + T) - (R^*x_2 + T^*)\|. \quad (10)$$

For convenience, we introduce ADD(S) metric:

$$\text{ADD(S)} = \begin{cases} \text{ADD} & \mathcal{O} \text{ is asymmetric} \\ \text{ADD-S} & \mathcal{O} \text{ is symmetric} \end{cases} \quad (11)$$

For LineMOD and Occlusion LineMOD datasets, we choose the threshold with 0.1d (10% of the objects diameter) to calculate the accuracy of ADD(S), following (Peng et al. 2019b; He et al. 2021). For YCB-Video dataset, following (Xiang et al. 2018; Wang et al. 2019; He et al. 2020, 2021), we calculate the AUC (area under the accuracy-threshold curve) of ADD(S) with a maximum threshold of 0.1 meters.

5D Anchor: Suitable for Different Direct Methods

Apply the 5D anchor to Uni6D and ES6D. To verify the extensibility of the proposed 5D anchor, we apply it to ES6D (Mo et al. 2022b) and Uni6Dv2. The original ES6D feeds cropped RGB images with normalized (x, y, z) and regresses the offsets of visible points to the centroid of a object. Since ES6D is not intended for the Occlusion LineMOD, we modify the code and use ES6D* to denote our implementation. To apply 5D anchor to ES6D*, we replace the visible points with one 5D anchor. The input is changed as $(RGB, \Delta U, \Delta V, \Delta X, \Delta Y, \Delta D, NRM)$ and the regression target is changed as the offset of the anchor to the centroid. The comparison results on Occlusion LineMOD are shown in Table 1. We can observe that using 5D anchor can significantly improve the performance of both Uni6Dv2 and ES6D. More implementation details are provided in supplementary materials.

5D Anchor with Sparse and Dense Predictions. Sparse and dense predictions are the common ways in 6D pose estimation. To demonstrate the generalization of the proposed 5D anchor, we conduct experiments on sparse and dense methods. Uni6Dv2 is chosen as the sparse method. The dense method is constructed by changing the RT head of Uni6Dv2 to the dense prediction head, since there are few direct methods that could be modified to the dense prediction way with anchor. We add 5D anchor to the above base-lines, then we feed $(RGB, \Delta U, \Delta V, \Delta X, \Delta Y, \Delta D, NRM)$ to networks as input. The comparison results on Occlusion LineMOD are shown in Table 2, using 5D anchor can significant improve the performance of both dense prediction (+38.7%) and sparse prediction (+62.6%) methods. We provide more implementation details in supplementary materials.

Uni6Dv3: Comparison with SOTA Methods

We provide comprehensive and detailed comparison results on Occlusion LineMOD, LineMOD, and YCB-Video

	Uni6Dv2	Uni6Dv2+5D anchor	ES6D*	ES6D*+5D anchor
Avg	40.6	79.3	71.5	75.0

Table 1: Evaluation results of different methods with 5D anchor on Occlusion LineMOD dataset. ES6D* denotes our implementation.

	Sparse	Sparse+5D anchor	Dense	Dense+5D anchor
Avg	40.6	79.3	12.6	75.2

Table 2: Evaluation results of sparse and dense prediction with 5D anchor on Occlusion LineMOD dataset.

datasets. For the brevity of the paper, category-level experimental results on YCB-Video are provided in Supplementary Materials.

Average Results. In order to comprehensively analyze the performance, we present the mean results of different methods on Occlusion LineMOD, LineMOD, and YCB-Video datasets in Table 3. Note that ES6D only officially reports results on YCB-Video dataset. Compared with existing methods, Uni6Dv3 achieves state-of-the-art on overall three datasets, outperforming FFB6D (He et al. 2021) by 3.9% (90.1 vs. 86.2). Moreover, compared to the Uni6Dv2, adding 5D anchor brings 13.7% (90.1 vs. 76.4) improvement, which proves the effectiveness of our 5D anchor mechanism.

Evaluation on Occlusion LineMOD Dataset. The quantitative results on Occlusion LineMOD dataset are presented in Table 4. Compared with the baseline Uni6Dv2, employing 5D anchor achieves a significant improvement (+38.7%) on ADD(S) metric and outperforms state-of-the-art method FFB6D (He et al. 2021) by 13.1%. Noteworthy, adopting 5D anchor makes the network be more reliable when there are significant translation distribution gap. Taking “eggbox” as an example, which has a variation translation distribution in Fig. 1(a), using 5D anchor in it achieves a significant improvement, from 4.6% to 96.5%, showing the location-invariant estimation ability of the proposed 5D anchor.

Evaluation on LineMOD Dataset. The quantitative results on LineMOD dataset are presented in Table 5. Compared with our baseline Uni6Dv2, introducing 5D anchor brings 2.3% performance gain on ADD(S), demonstrating the effectiveness of our 5D anchor mechanism. Compared to FFB6D (He et al. 2021), the performance gap is minimal (99.5 vs. 99.7), while our method has a more straightforward design and faster speed.

Uni6Dv3: Reducing Data Dependency

In this section, we use fewer training data to explore the advantage of the 5D anchor mechanism, that is, it minimizes the translation distribution gap of the dataset to reduce the convergence difficulty of the network. We randomly sample 1% and 10% of the training data from YCB-Video as new training datasets. As listed in Table 6, compared with the baseline Uni6Dv2, the proposed method exhibits better performance on both 1% (57.1 vs. 76.6) and 10% training data (79.7 vs. 86.5), and has better robustness in case of reduced

	PoseCNN	PVN3D	FFB6D	ES6D	Uni6D	Uni6Dv2	Ours
Occlusion LineMOD	24.9	63.2	66.2	-	30.7	40.6	79.3
LineMOD	88.6	99.4	99.7	-	97.0	97.2	99.5
YCB-Video	59.9	91.8	92.7	89.0	88.8	91.5	91.5
Avg	57.8	84.8	86.2	-	72.2	76.4	90.1

Table 3: Average results on three datasets. The metric on Occlusion LineMOD and LineMOD is the accuracy of ADD(S), and the metric on YCB-Video is AUC of ADD(S).

Method	PoseCNN	PVN3D	FFB6D	Uni6D	Uni6Dv2	Ours
ape	9.6	33.9	47.2	33.0	44.3	63.2
can	45.2	88.6	85.2	51.1	53.3	91.1
cat	0.9	39.1	45.7	4.6	16.7	64.4
driller	41.4	78.4	81.4	58.4	63.0	78.1
duck	19.6	41.9	53.9	34.8	51.6	62.6
eggbox	22.0	80.9	70.2	1.7	4.6	96.5
glue	38.5	68.1	60.1	30.2	40.3	95.8
holepuncher	22.1	74.7	85.9	32.1	50.9	82.5
Avg	24.9	63.2	66.2	30.7	40.6	79.3

Table 4: Evaluation results on the Occlusion LineMOD dataset. Symmetric objects are denoted in bold.

data volume. Especially, our method achieves comparable performance with full training data in ADD-S (94.9 vs. 96.6) when only using 10% training data. Since YCB-Video has a large amount of real training data with same pose distribution of test data, there is no obvious performance gain on 100% training data. The main reason for 5D anchor can greatly reduce the data dependency is that it makes the target distribution compact, easing the network regression learning. It is meaningful for practical 6d pose estimation applications where data collection and labeling are expensive.

Uni6Dv3: Ablation Study

In this section, we will analyze the effectiveness of the 5D anchor mechanism and compare different anchor generation strategies. All experiments are conducted on Occlusion LineMOD dataset.

Effectiveness of 5D Anchor. We analyze the effect of different anchor strategies, which include anchor on input, anchor on output, and our anchor on input and output in Table 7. First, we introduce anchor into input and output separately. The performance of anchor on input is limited

	PoseCNN	DenseFusion	PVN3D	FFB6D	Uni6D	Uni6Dv2	Ours
ape	77.0	92.3	97.3	98.4	93.7	95.7	98.2
benchvise	97.5	93.2	99.7	100.0	99.8	99.9	100.0
camera	93.5	94.4	99.6	99.9	96.0	95.8	99.6
can	96.5	93.1	99.5	99.8	99.0	96.0	99.9
cat	82.1	96.5	99.8	99.9	98.1	99.2	99.1
driller	95.0	87.0	99.8	100.0	99.1	99.2	99.8
duck	77.7	92.3	97.7	98.4	90.0	92.1	97.4
eggbox	97.1	99.8	99.8	100.0	100.0	100.0	100.0
glue	99.4	100.0	100.0	100.0	99.2	99.6	100.0
holepuncher	52.8	92.1	99.9	99.8	90.2	92.0	99.7
iron	98.3	97.0	99.7	99.9	99.5	98.0	100.0
lamp	97.5	95.3	99.8	99.9	99.4	98.5	99.9
phone	87.7	92.8	99.5	99.7	97.4	97.7	99.8
Avg	88.6	94.3	99.4	99.7	97.0	97.2	99.5

Table 5: Evaluation results on the LineMOD dataset. Symmetric objects are denoted in bold.

Training data ratio	Uni6Dv2		Ours	
	ADD-S	ADD(S)	ADD-S	ADD(S)
100%	96.8	91.5	96.6	91.5
10%	92.5	79.7	94.9	86.5
1%	79.1	57.1	91.9	76.6

Table 6: The advantage of reducing the amount of training data on the YCB-Video dataset.

Relative Input to the Anchor	Relative Output to the Anchor	ADD(S)
✓		40.6
	✓	17.8
✓	✓	63.9
		79.3

Table 7: Comparison of 5D anchor design.

because the network is difficult to regress the absolute position from relative input. Meanwhile, the performance of anchor on output achieves 23% improvement over the baseline by reducing the translation distribution gap with the offset regression. However, according to the projection equation, there is still a mismatch between absolute input and relative output. Thus, only adding anchor to the output can not achieve ideal results. To further analyze the impact of the 5D anchor, we introduce it into both input and output following the projection equation, achieve the best results with 38.7% improvement in Table 7. To summarize, the proposed 5D anchor, added to the input and output, can solve the distribution gap problem while obeying the projection equation and achieving state-of-the-art results.

5D anchor generation strategies. To build a stable 5D anchor, we attempt three different anchor generation strategies, as shown in Table 8. The first one selects a visible point (u_0, v_0, d_0) with a depth value closest to the object’s mean depth, which can ensure the anchor point is under the surface. The value of x_0 and y_0 are further calculated from (u_0, v_0, d_0) based on Eq 3. However, unstable UV values of 5D anchor make the network learning tougher. The second strategy fixes the UV value as the center of the ROI region, the nearest point’s depth as anchor depth, and then calculates x_0 and y_0 based on Eq 3. Compared with the first one, the UV offset is easy to learn, and the improvement is significant (63.4 vs. 73.5). However, due to the occlusion or the irregular shape, the center of the ROI may be a background pixel, and the nearest depth could be a noise point from the sensor or background. Therefore, we adopt the mean depth value of the object region as the anchor depth, which improves the stability of 5D anchor in 2D image plane and 3D space, achieving the best result.

Visualization

Visualization results of Occlusion LineMOD dataset are shown in Fig. 4. We can observe that Uni6Dv3 could predict a more precise and robust 6D pose on the heavily occluded objects compared to other methods. Moreover, benefiting from 5D anchor, the orientation of objects with only

u_0 and v_0	5D Anchor Generation Strategies		ADD(S)
	x_0 and y_0	d_0	
Default values	mean of visible points	mean of visible points	63.4
ROI center	Default values	nearest depth point	73.5
ROI center	Default values	mean depth point	79.3

Table 8: Comparison of generation strategies for 5D anchor $(u_0, v_0, x_0, y_0, d_0)$. “Default values” can be calculated based on Eq 3.

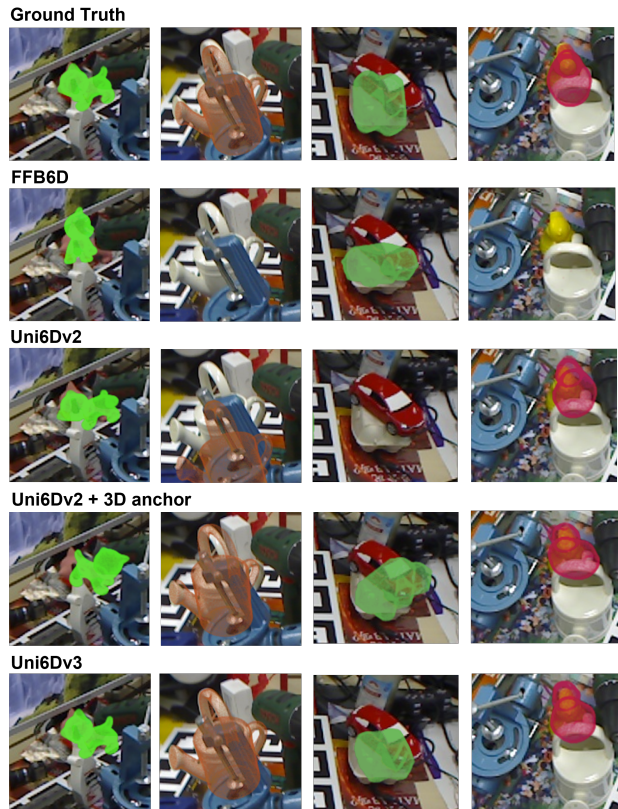


Figure 4: Qualitative results of 6D pose estimation on the Occlusion LineMOD dataset.

a few visible points is correctly predicted, which proves that the proposed anchor improves the robustness and generalization of the network.

Conclusion

In this paper, we present the benefits of introducing anchor mechanism in 6D pose estimation, i.e., reshaping the distribution of regression target, and uncover the mismatch issue between absolute input and relative output when utilizing an anchor in the regression. An anchor-based projection model is derived from the projection equation and the 5D anchor is naturally proposed. Various anchor generation strategies are evaluated and the optimal one is applied to different direct methods, such as Uni6Dv2 and ES6D. Experiments demonstrate that Uni6Dv3, which is produced by applying the 5D anchor to Uni6Dv2, achieves state-of-the-art on three bench-

mark datasets. Furthermore, the proposed method greatly reduces the demand of training data, which is crucial in practice.

We believe that 5D anchor mechanism is able to inspire other 3D tasks, such as category-level pose estimation, 3D reconstruction, 3D object detection with RGB-D or Lidar data, since the underlying data input of these 3D task inherently follows projection constraint.

References

- Brachmann, E.; Krull, A.; Michel, F.; Gumhold, S.; Shotton, J.; and Rother, C. 2014. Learning 6d object pose estimation using 3d object coordinates. In *European conference on computer vision*, 536–551.
- Calli, B.; Singh, A.; Walsman, A.; Srinivasa, S.; Abbeel, P.; and Dollar, A. M. 2015. The ycb object and model set: Towards common benchmarks for manipulation research. In *2015 international conference on advanced robotics (ICAR)*, 510–517.
- Chen, X.; Ma, H.; Wan, J.; Li, B.; and Xia, T. 2017. Multi-view 3d object detection network for autonomous driving. In *Proceedings of the IEEE conference on Computer Vision and Pattern Recognition*, 1907–1915.
- Geiger, A.; Lenz, P.; and Urtasun, R. 2012. Are we ready for autonomous driving? the kitti vision benchmark suite. In *2012 IEEE conference on computer vision and pattern recognition*, 3354–3361.
- Haugaard, R. L.; and Buch, A. G. 2022. SurfEmb: Dense and Continuous Correspondence Distributions for Object Pose Estimation with Learnt Surface Embeddings. In *Proceedings of the IEEE/CVF Conference on Computer Vision and Pattern Recognition*, 6749–6758.
- He, K.; Gkioxari, G.; Dollár, P.; and Girshick, R. 2017. Mask R-CNN. In *Proceedings of the IEEE international conference on computer vision*, 2961–2969.
- He, Y.; Huang, H.; Fan, H.; Chen, Q.; and Sun, J. 2021. Ffb6d: A full flow bidirectional fusion network for 6d pose estimation. In *Proceedings of the IEEE/CVF Conference on Computer Vision and Pattern Recognition*, 3003–3013.
- He, Y.; Sun, W.; Huang, H.; Liu, J.; Fan, H.; and Sun, J. 2020. Pvn3d: A deep point-wise 3d keypoints voting network for 6dof pose estimation. In *Proceedings of the IEEE/CVF conference on computer vision and pattern recognition*, 11632–11641.
- Hinterstoisser, S.; Holzer, S.; Cagniart, C.; Ilic, S.; Konolige, K.; Navab, N.; and Lepetit, V. 2011. Multimodal templates for real-time detection of texture-less objects in heavily cluttered scenes. In *2011 international conference on computer vision*, 858–865.
- Hodan, T.; Barath, D.; and Matas, J. 2020. Epos: Estimating 6d pose of objects with symmetries. In *Proceedings of the IEEE/CVF conference on computer vision and pattern recognition*, 11703–11712.
- Jiang, X.; Li, D.; Chen, H.; Zheng, Y.; Zhao, R.; and Wu, L. 2022. Uni6D: A Unified CNN Framework without Projection Breakdown for 6D Pose Estimation. *IEEE/CVF Conference on Computer Vision and Pattern Recognition (CVPR)*.
- Kiru, P.; Patten, T.; and Pix2Pose, M. 2019. Pixel-Wise Coordinate Regression of Objects for 6D Pose Estimation. *Proceedings of the ICCV, Seoul, Korea*, 27–28.
- Lang, A. H.; Vora, S.; Caesar, H.; Zhou, L.; Yang, J.; and Beijbom, O. 2019. Pointpillars: Fast encoders for object detection from point clouds. In *Proceedings of the IEEE/CVF conference on computer vision and pattern recognition*, 12697–12705.
- Li, Y.; Wang, G.; Ji, X.; Xiang, Y.; and Fox, D. 2018. Deepim: Deep iterative matching for 6d pose estimation. In *Proceedings of the European Conference on Computer Vision (ECCV)*, 683–698.
- Li, Z.; Wang, G.; and Ji, X. 2019. Cdpn: Coordinates-based disentangled pose network for real-time rgb-based 6-dof object pose estimation. In *Proceedings of the IEEE/CVF International Conference on Computer Vision*, 7678–7687.
- Mo, N.; Gan, W.; Yokoya, N.; and Chen, S. 2022a. ES6D: A Computation Efficient and Symmetry-Aware 6D Pose Regression Framework. In *Proceedings of the IEEE/CVF Conference on Computer Vision and Pattern Recognition*, 6718–6727.
- Mo, N.; Gan, W.; Yokoya, N.; and Chen, S. 2022b. ES6D: A Computation Efficient and Symmetry-Aware 6D Pose Regression Framework. *arXiv preprint arXiv:2204.01080*.
- Peng, S.; Liu, Y.; Huang, Q.; Zhou, X.; and Bao, H. 2019a. Pvnnet: Pixel-wise voting network for 6dof pose estimation. In *Proceedings of the IEEE/CVF Conference on Computer Vision and Pattern Recognition*, 4561–4570.
- Peng, S.; Liu, Y.; Huang, Q.; Zhou, X.; and Bao, H. 2019b. Pvnnet: Pixel-wise voting network for 6dof pose estimation. In *Proceedings of the IEEE/CVF Conference on Computer Vision and Pattern Recognition*, 4561–4570.
- Rad, M.; and Lepetit, V. 2017. Bb8: A scalable, accurate, robust to partial occlusion method for predicting the 3d poses of challenging objects without using depth. In *Proceedings of the IEEE international conference on computer vision*, 3828–3836.
- Ren, S.; He, K.; Girshick, R.; and Sun, J. 2015. Faster r-cnn: Towards real-time object detection with region proposal networks. *Advances in neural information processing systems*, 28.
- Su, Y.; Saleh, M.; Fetzer, T.; Rambach, J.; Navab, N.; Busam, B.; Stricker, D.; and Tombari, F. 2022. ZebraPose: Coarse to Fine Surface Encoding for 6DoF Object Pose Estimation. In *Proceedings of the IEEE/CVF Conference on Computer Vision and Pattern Recognition*, 6738–6748.
- Sun, M.; Zheng, Y.; Bao, T.; Chen, J.; Jin, G.; Zhao, R.; Wu, L.; and Jiang, X. 2022. Uni6Dv2: Noise Elimination for 6D Pose Estimation. *arXiv preprint arXiv:2208.06416*.
- Wang, C.; Xu, D.; Zhu, Y.; Martín-Martín, R.; Lu, C.; Fei-Fei, L.; and Savarese, S. 2019. Densefusion: 6d object pose estimation by iterative dense fusion. In *Proceedings of*

the IEEE/CVF conference on computer vision and pattern recognition, 3343–3352.

Wang, G.; Manhardt, F.; Shao, J.; Ji, X.; Navab, N.; and Tombari, F. 2020. Self6d: Self-supervised monocular 6d object pose estimation. In *European Conference on Computer Vision*, 108–125. Springer.

Wang, G.; Manhardt, F.; Tombari, F.; and Ji, X. 2021. Gdr-net: Geometry-guided direct regression network for monocular 6d object pose estimation. In *Proceedings of the IEEE/CVF Conference on Computer Vision and Pattern Recognition*, 16611–16621.

Xiang, Y.; Schmidt, T.; Narayanan, V.; and Fox, D. 2018. PoseCNN: A Convolutional Neural Network for 6D Object Pose Estimation in Cluttered Scenes. In *Robotics: Science and Systems (RSS)*.

Xu, D.; Anguelov, D.; and Jain, A. 2018. Pointfusion: Deep sensor fusion for 3d bounding box estimation. In *Proceedings of the IEEE conference on computer vision and pattern recognition*, 244–253.

Zhou, Y.; and Tuzel, O. 2018. Voxelnet: End-to-end learning for point cloud based 3d object detection. In *Proceedings of the IEEE conference on computer vision and pattern recognition*, 4490–4499.